Journal of Biomechanics 161 (2023) 111868

Contents lists available at ScienceDirect

Journal of Biomechanics

journal homepage: www.elsevier.com/locate/jbiomech

Biaxial stretch can overcome discrepancy between global and local orientations of wavy collagen fibres

Michaela Turčanová [a,*], Jiří Fischer [a], Markéta Hermanová [b], Zdeněk Bednařík [b], Pavel Skácel [a], Jiří Burša [a]

[a] Brno University of Technology, Faculty of Mechanical Engineering, Institute of Solid Mechanics, Mechatronics and Biomechanics, Technická 2896/2, Brno 616 69, Czech Republic

[b] 1st Department of Pathology, St. Anne's University Hospital Brno and Faculty of Medicine, Masaryk University, Pekařská 664/53, 656 91 Brno, Czech Republic

ARTICLE INFO

Keywords:
Arterial wall
Collagen
Fibre direction
Fibre waviness
Concentration parameter

ABSTRACT

Most frequently used structure-based constitutive models of arterial wall apply assumptions on two symmetric helical (and dispersed) fibre families which, however, are not well supported with histological findings where two collagen fibre families are seldom found. Moreover, bimodal distributions of fibre directions may originate also from their waviness combined with ignoring differences between local and global fibre orientations. In contrast, if the model parameters are identified without histological information on collagen fibre directions, the resulting mean angles of both fibre families are close to ±45°, which contradicts nearly all histologic findings. The presented study exploited automated polarized light microscopy for detection of collagen fibre directions in porcine aorta under different biaxial extensions and approximated the resulting histograms with unimodal and bimodal von Mises distributions. Their comparison showed dominantly circumferential orientation of collagen fibres. Their concentration parameter for unimodal distributions increased with circumferential load, no matter if acting uniaxially or equibiaxially. For bimodal distributions, the angle between both dominant fibre directions (chosen as measure of fibre alignment) decreased similarly for both uniaxial and equibiaxial loads. These results indicate the existence of a single family of wavy circumferential collagen fibres in all layers of the aortic wall. Bimodal distributions of fibre directions presented sometimes in literature may come rather from waviness of circumferentially arranged fibres than from two symmetric families of helical fibres. To obtain a final evidence, the fibre orientation should be analysed together with their waviness.

1. Introduction

Anisotropy of arterial wall, its strain stiffening and strength are related to organization of collagen fibres (Gasser et al., 2012; Geest et al., 2006; Sassani et al., 2015), the knowledge of which is crucial for structure-based constitutive models of such tissues (Holzapfel et al., 2015). These models can improve, for instance, computational assessment of rupture risk of aortic aneurysms or atherosclerotic plaques and correct timing of respective surgeries (Akyildiz et al., 2014; Gasser et al., 2012; Hoffman et al., 2017; Polzer et al., 2020).

Anisotropic constitutive models of arterial tissue formulated within last decades are mostly based on some assumptions on distribution of collagen fibres. First, two symmetric helical perfectly aligned fibre families were postulated in HGO model (Holzapfel et al., 2000), with circumferential and axial fibre families added to them in the four fibre family model (e.g., (Ferruzzi et al., 2011)). More advanced published models based on angular integration approach (initiated by (Lanir, 1983), and followed by many others) considered continuous distributions of fibre directions. Other implementation strategy tries to approximate fibre dispersion through generalized structure tensor, e.g. GOH model (Gasser et al., 2006). Some recent models strive for consideration of waviness of collagen fibres approximated, for instance, with a log-logistic probability distribution function (Agianniotis et al., 2011) or a triangular one (Martufi & Gasser, 2011); the varying stretch at which the fibres straighten is sometimes explained through proteoglycan bridges interconnecting individual collagen fibrils. (Grytz & Meschke, 2009) used a three-dimensional cylindrical helix to represent the substructure at a fibrillar level while (Marino et al., 2018) introduced even intermolecular cross-links stiffness density and molecular persistence length as structural features of their model. Such resolution

* Corresponding author.
E-mail address: turcanova@fme.vutbr.cz (M. Turčanová).

https://doi.org/10.1016/j.jbiomech.2023.111868
Accepted 9 November 2023
Available online 11 November 2023

level, however, is too high for computational simulations of whole arteries where the models with dispersed fibre directions within a few fibre families and phenomenological (exponential) fibre response are preferred. They need two structural parameters for each fibre family: the mean orientation of fibres and the dispersion (or concentration). Knowledge on fibre arrangement is critical for these models; if the structural parameters are identified purely from mechanical responses of arterial wall, they lose their structural background and may be in contradiction to histological findings (Gaul et al., 2017; Polzer et al., 2015; Schrauwen et al., 2012). Nevertheless, a lack of structural information on collagen fibre arrangement in pathological and healthy arteries represents still a limiting factor in structure-based constitutive modelling of arterial tissues (Fischer et al., 2023; Haskett et al., 2010).

There are various approaches to obtain the orientation and dispersion of collagen fibres, e.g. small-angle X-ray scattering (Guinier et al., 1955), confocal laser scanning microscopy (Schrauwen et al., 2012), multiphoton microscopy (Tsamis et al., 2013), second harmonic generation (SHG) (Schriefl et al., 2013), quantitative polarized light microscopy (Low et al., 2015), or small-angle light scattering (Gaul et al., 2017). Nevertheless, polarized light microscopy (PLM) has been most widely used (Finlay et al., 1998; Gasser et al., 2012; Rowe et al., 2003; Sáez et al., 2016; Schriefl, Zeindlinger, et al., 2012; Wicker et al., 2008) and an automatic algorithm enables now to obtain histograms based on large datasets (typically $\approx 5.10^5$ measured pixels) (Turčanová et al., 2021). Although these histograms are often interpreted as two fibre families in the arterial wall, not always their existence is well substantiated. Frequently a bimodal distribution is preferred due to assumptions of the applied constitutive model without a rigorous comparison with any other distributions (Gasser et al., 2012; Haskett et al., 2010; Sassani et al., 2015; Schrauwen et al., 2012).

Moreover, the pointwise evaluation of fibre directions (intrinsic for PLM and most of the above-mentioned methods) gives information on local rather than global fibre directions needed for the constitutive models. However, some recent studies indicate the relation between local and global fibre directions could be solved by analysing the distribution of fibre directions under load eliminating the effects of waviness (Rezakhaniha et al., 2012; Gaul et al., 2017; Schrauwen et al., 2012; Schriefl, Zeindlinger, et al., 2012). The more the fibres are stretched the more the local fibre directions (tangent to fibre contour) coincide with the global ones (line connecting fibre endpoints) as depicted in Figure S1 in Supplementary material. Therefore, we investigated changes in the distribution of collagen fibres orientation in porcine aortic wall under different loading states and compared different approximations of the obtained histograms.

2. Materials and methods

Although many authors apply primarily a bimodal distribution to approximate the experimentally obtained histograms of collagen fibre directions in the arterial wall, it is seldom well supported and unimodal or other distributions give often comparable (or the same) goodness of the fit (Fischer & Bursa, 2019; Gaul et al., 2017; Schrauwen et al., 2012). Another part of the presented bimodal distributions may be attributed rather to tissue non-homogeneity, either to different orientation in individual layers of arterial wall (Schriefl, Reinisch, et al., 2012) or another non-homogeneity in the investigated tissue (Jett et al., 2020). It was also shown that even one family of wavy fibres may result in a bimodal histogram of local directions which may be easily misinterpreted as two fibre families with different global directions (Novák et al., 2015).

Our preliminary testing in radial compression (described separately in the Supplementary material) investigated the fibre distribution in out-of-plane sections and showed — in accordance with the literature (Schrauwen et al., 2012; Schriefl, Reinisch, et al., 2012) — a single fibre family with circumferential and axial orientation in circumferential-radial and axial-radial sections, respectively. The mean orientation of fibres was independent of the load while the relatively small dispersion in radial direction decreased with increasing load (see Figures S3 and S4 and Table S1). However, in these experiments we did not know the stretches in the circumferential-axial plane and also evaluation of fibre directions in this plane was impossible due to very limited penetration of the dye between the glasses (see Figure S2). Therefore, these results were used only to present a complete 3D distribution of fibre directions (see Fig. 2); this should be known because the GOH model assumes their axial symmetric distribution in each family. Therefore, the experiments in biaxial tension presented below focus on distributions of fibre directions in the circumferential-axial plane. In contrast, they disable evaluation of the out-of-plane sections because the faces of the specimen are damaged by fixation hooks used for specimen extension.

2.1. Histological slices under biaxial tensile loads

Samples of porcine aortas for histological analyses were harvested in a local slaughterhouse from 10 months old pigs weighting 105–120 kg. Specimens were cleaned of excess surrounding tissue, their circumferential and axial directions were marked, and subjected to biaxial extension (see Fig. 1). The deformed specimens were fixed in 10 % formaldehyde solution at room temperature for 24 h and then embedded in paraffin. Microtome (Leica SM2010 R) was used to cut 5 μm thick slices. Finally, every slice was stained using 0.1 % Picro Sirius Red to emphasize the needed collagen birefringence (see (Novák et al., 2015; Turčanová et al., 2021) for details). The quality of slices was afterwards checked under a light microscope by a pathologist, who also evaluated the composition of the wall with regard to the presence of tunica media and tunica adventitia in the axial and circumferential axis within separate samples taken from edges of the specimens.

To clarify the load dependent changes in fibre arrangement in circumferential-axial plane, the specimens were investigated, in addition to the unloaded state, under different levels of biaxial extension (up to 32 %). Therefore, a single-purpose fixture has been designed (see Fig. 1) enabling us immersion of the specimen under specific biaxial extension in formaldehyde for specimen fixation. This cannot be done with a standard biaxial testing machine due to toxicity of formaldehyde. Here stretches (axial and circumferential independently) were set manually with screws, symmetrically to the specimen centre and

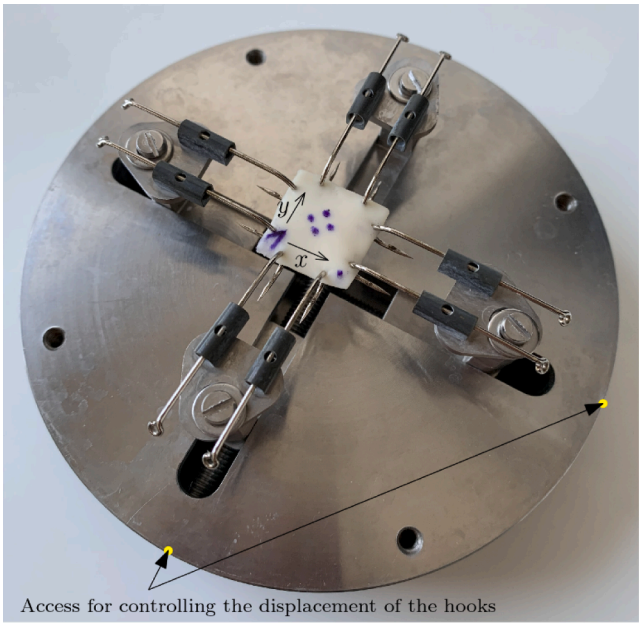

Fig. 1. Fixture with the specimen to be fixed in formaldehyde (here in the unloaded state). Circumferential and axial directions are specified as x and y, respectively.

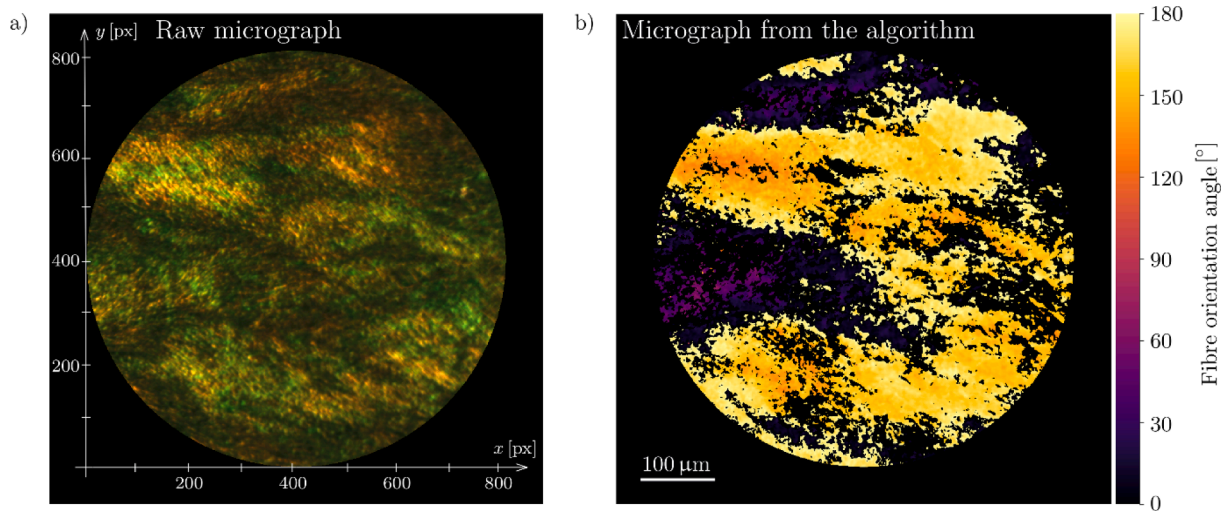

Fig. 2. Example of evaluation of fibre directions. Left image shows a raw micrograph with setting for green color and perpendicular polarizers. Right image shows the same micrograph with directions (in colour scale) evaluated by the proposed algorithm in each pixel, which are then transformed into histograms. The black areas are created by the pixels in which the collagen fibres were not visible and the direction could not be evaluated. (For interpretation of the references to color in this figure legend, the reader is referred to the web version of this article.)

evaluated optically through displacements of ink markers (see Fig. 1) captured by a CCD camera (Basler, sCA1300-32gm, monochromatic) with pixel size of 0.039 mm. The applied software Tibixus calculates stretch components with sub-pixel accuracy of approximately 0.001. On the contrary, due to interference between stretch components (Poisson's effect) and direct control of grip displacements without any feedback, the accuracy of reaching the required state of strain (equibiaxial, for instance) was lower (see Table 1). Therefore, all cases with both stretches differing by 0.02 (2 % strain) or less were considered as *equibiaxial*. The other cases are denoted bellow as *circumferentially-dominated* or *axially-dominated* biaxial loads.

2.2. Evaluation of directions of collagen fibres and their dispersion

All the histological slices were scanned with an upright polarized light microscope (Padim, Drexx s.r.o., CZ) in a transmission configuration equipped with a digital camera (Bresser GmbH, Germany) and standard 2D rotary stage (Padim, Drexx s.r.o., CZ). All images were recorded under identical illumination and magnification (5 × objective, numerical aperture 0.12; 10 × ocular); the trimmed images had the size of 960 × 960 pixels (pixel size 0.73 µm). Two sets per six images recorded with crossed and deflected polarizers were evaluated using the automatic algorithm (using MATLAB R2020b) giving the fibre directions in each pixel (see Fig. 2). This local fibre directions throughout all the image were then transformed into raw histograms of directions in Fig. 3 and Fig. 4. See (Turčanová et al., 2021) for more details.

2.3. Fitting of histological data

The structural parameters needed for the constitutive models, i.e. mean orientation and dispersion of collagen fibre families, were obtained by fitting the histograms from histological analyses with unimodal and bimodal von Mises probability distribution functions given by eq. (1) (Gasser et al., 2006):

$$\rho(\Theta) = \sum_{i=1}^{N} \frac{1}{N \bullet \pi I_0(b_i)} e^{b_i \cos(2\bullet(\Theta-\mu_i))}, \tag{1}$$

where b_i is the concentration parameter, Θ is the fibre angle, μ is the mean angle of the fibre family and I_0 is a Bessel function of first kind of order zero. The number of fibre families $N = 1$ and 2 defines unimodal and bimodal distributions, respectively, and the index i denotes the i^{th} fibre family.

The fitting procedure was performed in Curve Fitting Toolbox in MATLAB with user defined functions; mean angles μ_i and concentration parameters b_i of fibre families were obtained using non-linear least square method to fit the obtained histograms with eqs. (1) and (2) for unimodal and bimodal distributions, respectively. Coefficient of determination R^2 was used as quality criterion of the fit. For comparison of mean angles obtained using different distributions, the bimodal distribution was recalculated into the middle angle $\omega=(\mu_1 + \mu_2)/2$ representing the average of both mean directions and into the span angle $\phi = abs(\mu_1-\mu_2)$ between them; the latter represents a measure of fibre alignment with the acting load better than concentration parameters b_1 and b_2. The dispersion parameter κ, used preferably in some constitutive models, can be evaluated from concentration parameter b with the following equation (Gasser et al., 2006):

$$\kappa = \int_0^{\pi} \rho(\Theta)\sin^3(\Theta)d\Theta. \tag{3}$$

Let's notice that $b = 0$ and $\kappa = 1/3$ for isotropic distribution of fibre

Table 1
Classification of samples according to the applied load.

Circumferentially dominated			Axially dominated			Equibiaxial		
Sample No.	λ_x [-]	λ_y [-]	Sample No.	λ_x [-]	λ_y [-]	Sample No.	λ_x [-]	λ_y [-]
1AO 1	1.10	1.07	1AO 2	1.06	1.10	1AO 3	1.06	1.06
2AO 1	1.07	0.99	2AO 2	1.01	1.21	1AO 4	1.15	1.17
2AO 9	1.25	0.98	2AO 8	0.99	1.23	2AO 3	1.13	1.14
3AO 1	1.13	1.09	3AO 2	1.03	1.18	2AO 7	1.12	1.11
3AO 5	1.14	1.02	3AO 3	1.15	1.19	3AO 8	1.17	1.16
			3AO 7	1.00	1.32			

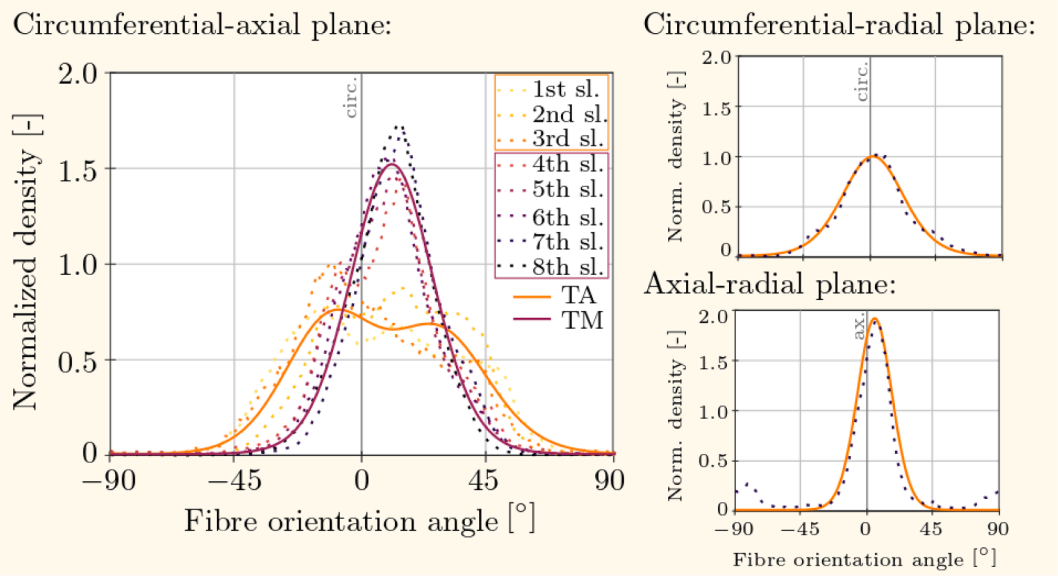

Fig. 3. The resulting histograms for all slices of the first aorta in the unloaded state (1AO 1). Raw histograms from all the evaluated planes and sections are depicted as dots while solid lines represent the distribution functions. In the circumferential-axial plane, the individual slices are ordered from the outer to the inner surface and the von Mises distribution functions are presented commonly for TA (orange) and TM (purple). (For interpretation of the references to color in this figure legend, the reader is referred to the web version of this article.)

orientations, and $b \to \infty$ and $\kappa \to 0$ for perfectly aligned fibres.

2.4. Statistical analyses

A group of analyses of statistical significance tests (with the level of significance $\alpha = 0.05$) were performed in software Minitab 15 using one-way ANOVA function. The data normality was verified by Kolmogorov–Smirnov test in Minitab 15 before performing the ANOVA analysis. For unimodal distributions, concentration parameter b and mean direction μ were used while for bimodal distributions, a similar comparison was done for the middle angle ω and the span angle $\boldsymbol{\Phi}$.

3. Results

3.1. Results of analyses under biaxial tension

The histological slices in circumferential-axial plane were typically 18 × 18 mm, therefore 9 evaluated microscopic regions (ca 4 × 4 mm^2) gave sufficient data (≈5.10^5 measured pixels) for histograms. Examples of raw histograms for individual slices of aorta No. 1 and the related distributions are shown in Fig. 3 for the unloaded state and in Fig. 4 for different loads. For the approximation curves, more than one half of the investigated slices at the inner surface are denoted as tunica media (TM) and the remaining outer layers as tunica adventitia (TA). In our previous study (Fischer et al., 2023) we have confirmed histologically that media creates more than one half of the thickness of porcine aorta and within a limited number of investigated slices (≤8) this criterion was mostly sufficient for assignment of slices to layers. For the number of slices > 6, moreover, we tested that shifts of the layer interface by one slice inwards or outwards showed insignificant effect on the resulting distributions in these layers. Complete data of all the tested aortas can be found in the Supplementary material (Figures S5, S6 and S7).

The samples were sorted according to deformation into four groups: unloaded (13 specimens), circumferentially dominated (5 sp.), axially dominated (6 sp.) direction, and equibiaxially loaded (5 sp.). Biaxial stretches for all the loaded samples are in Table 1.

The detailed results for all the specimens are presented in Tables S2 and S3 in Supplementary material where the preferred distribution is highlighted in bold. As the goodness of bimodal distribution is never worse than of the unimodal one, we preferred unimodal distribution if both distributions gave $R^2 > 0.9$ and if simultaneously the R^2 difference between both distributions was lower than 0.05. Bimodal distribution exhibited higher goodness in TA, in contrast to TM where unimodal distribution was preferred, (especially in cases loaded in the dominant fibre direction). The results are summarized in Table 2 and Table 3.

As concerns distribution of fibre directions in different planes, the concentration parameter b was the lowest in the circumferential-radial and the highest in the axial-radial plane, but the increase of b with increasing load was similar in all the three planes. The fibre orientation was (with a few exceptions) close to the circumferential direction and we found no impact of the load on the mean fibre orientation. In the circumferential-axial plane, parameters of both unimodal and bimodal distributions were used for comparison under different loads. For unimodal distributions, the concentration parameter b increased for the circumferentially dominated loads as well as for equibiaxial loads and this tendency was confirmed also by their increasing R^2. In contrast, the b parameter did not change significantly with the load acting axially, i.e. perpendicularly to the dominant fibre direction. These tendencies were found statistically significant in the whole aortic wall (all layers together – see Table 4). Within the separated TA and TM layers the significance was not confirmed (see Tables S4 and S5 in the Supplementary material); it was probably due to low numbers of samples because some values were very close to the limit of $p = 0.05$. Similar analyses of the span angle (between both fibre families) Φav in bimodal distributions gave statistically significant differences between all groups except for the unloaded vs. axially dominated specimens and the circumferentially dominated vs. equibiaxially loaded specimens.

4. Discussion

Our histological analyses confirmed no effect of the load on the mean direction of fibres being dominantly circumferential in most cases. Some higher deviations from this direction occurring more often in the TA (e.g. samples 3AO 0, 4AO 1, 2AO 8, 3AO 7 in Table S2) were related to lower goodness of the unimodal fit. The dominantly circumferential direction was confirmed by bimodal distributions for which the middle angle ω of the two fibre families remained always nearly zero. On the other hand, the tendency to higher fibre concentration with increasing

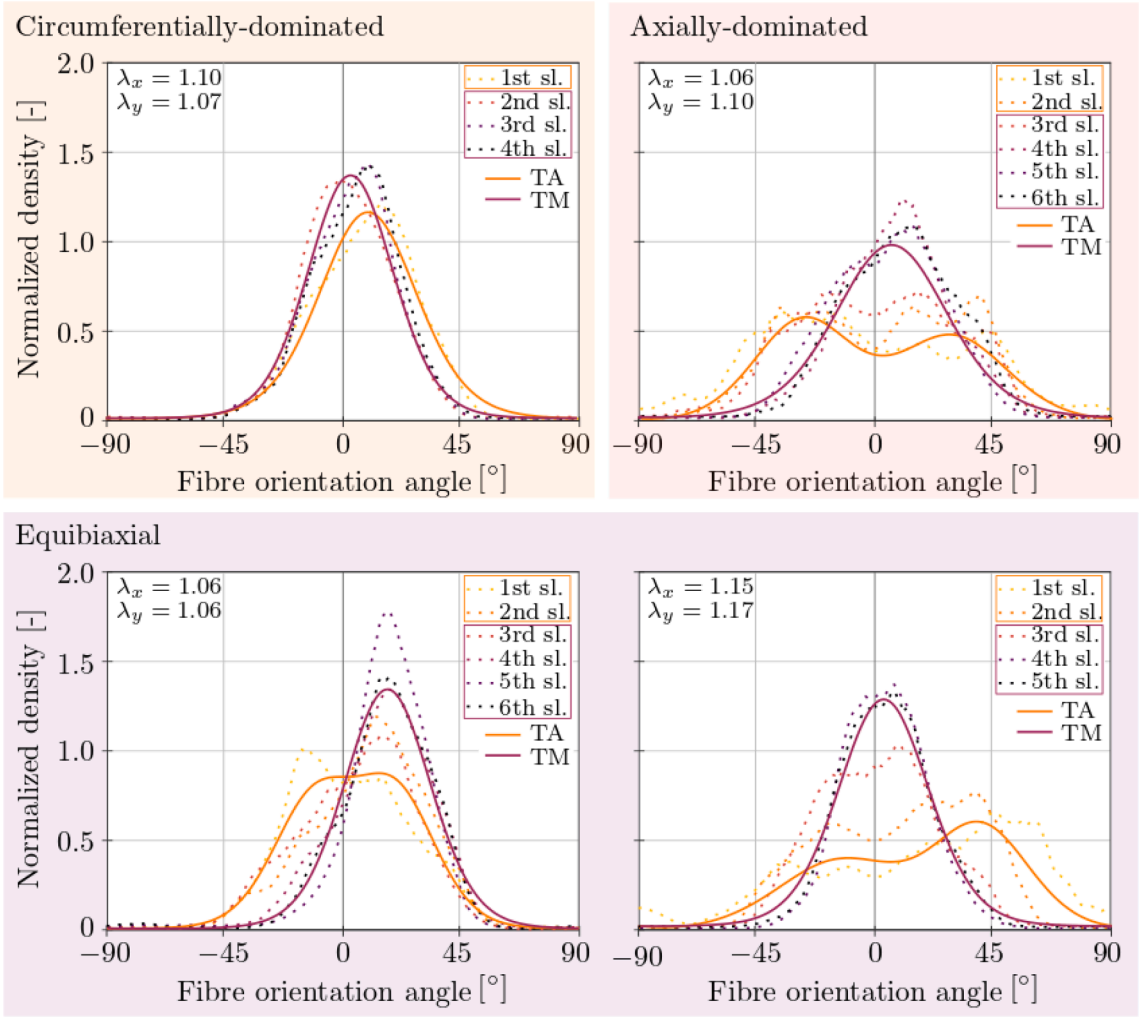

Fig. 4. The resulting histograms in the circumferential-axial plane for all the slices of the first aorta (1AO) under different biaxial loads. Raw histograms from all the evaluated sections are depicted as dots, the individual slices are ordered from the outer to the inner surface. The von Mises distribution functions are presented as solid lines common for TA (orange) and TM (purple). (For interpretation of the references to color in this figure legend, the reader is referred to the web version of this article.)

Table 2
Parameters of unimodal and bimodal distributions in circumferential-axial plane in TA for all samples. Zero angle corresponds to the circumferential direction, μ denotes the mean angle of the unimodal distribution, b its concentration parameter, ω the middle of both fibre families of the bimodal distribution and ϕ the angle between their mean directions. Subscripts av denote the average values for the groups with their standard deviations SD.

TA				
Load	**Unimodal**		**Bimodal**	
	$\mu_{av} \pm SD$ [°]	$b_{av} \pm SD$ [-]	$\omega_{av} \pm SD$ [°]	$\Phi_{av} \pm SD$ [°]
Unloaded	−14.1 ± 29.0	0.82 ± 0.36	3.3 ± 5.6	64.7 ± 22.7
Circ.-dominated	4.8 ± 4.7	1.56 ± 0.63	5.9 ± 4.5	35.4 ± 9.8
Axially-dominated	12.0 ± 40.0	0.89 ± 0.51	4.5 ± 4.8	62.0 ± 22.8
Equibiaxial	3.1 ± 13.3	1.28 ± 0.55	3.4 ± 7.1	42.8 ± 14.7

circumferential stretch was found, no matter whether this stretch was induced by uniaxial, biaxial or even equibiaxial extension (or radial compression – see Supplementary material). Only for axially-dominated biaxial loads (transversal to the mean fibre direction) the impact of load was insignificant. For bimodal distributions, a similar effect occurred for the span angle $\boldsymbol{\Phi}$ between both fibre families representing a deviation of

Table 3
Parameters of unimodal and bimodal distributions in TM in circumferential-axial plane for all samples. Zero angle corresponds to the circumferential direction. Angle μ denotes the mean angle of the unimodal distribution, b its concentration parameter, ω the middle of both fibre families of the bimodal distribution and ϕ the angle between their mean directions. Subscripts av denote the average values for the groups with their standard deviations SD. TA + TM represents the values averaged throughout both media and adventitia layers together.

	TM				TA + TM
Load	**Unimodal**		**Bimodal**		**Unimodal**
	$\mu_{av} \pm SD$ [°]	$b_{av} \pm SD$ [-]	$\omega_{av} \pm SD$ [°]	$\Phi_{av} \pm SD$ [°]	$b_{av} \pm SD$ [-]
Unloaded	0.4 ± 21.4	1.2 ± 0.97	4.4 ± 8.7	53.5 ± 20.9	1.03 ± 0.71
Circ.-dominated	0.3 ± 9.9	2.03 ± 0.85	1.0 ± 8.6	28.2 ± 7.6	1.77 ± 0.73
Axially-dominated	5.2 ± 19.4	1.3 ± 0.57	10.1 ± 6.9	45.1 ± 21.9	1.08 ± 0.55
Equibiaxial	3.2 ± 11.6	2.22 ± 0.76	3.4 ± 9.2	24.8 ± 9.5	1.75 ± 0.80

Table 4
Calculated statistical significance of differences between groups for concentration parameter b of the unimodal distribution and the angle between both fibre families Φav in bimodal distribution within the whole aortic wall. For statistically significant differences the p-value is highlighted in bold.

p-value: b	Unloaded	Circ.-dominated	Axially-dominated	Equibiaxial
Unloaded	–	**0.010**	0.726	**0.010**
Circ.-dominated	**0.010**	–	**0.027**	0.963
Axially-dominated	0.726	**0.027**	–	**0.036**
Equibiaxial	**0.010**	0.963	**0.036**	–
p-value: Φav	**Unloaded**	**Circ.-dominated**	**Axially-dominated**	**Equibiaxial**
Unloaded	–	**0.002**	0.527	**0.002**
Circ.-dominated	**0.002**	–	**0.018**	0.894
Axially-dominated	0.527	**0.018**	–	**0.027**
Equibiaxial	**0.002**	0.894	**0.027**	–

fibres orientation from the circumferential direction.

To illustrate the changes in fibre orientation under uniaxial load between helical and wavy fibres, a simple mathematical model is presented in the Supplementary material (S1). It is applied for the fibre angles of 40°, 45°, and 50° obtained typically when fitting the GOH or HGO models to experimental data without histological information on fibre directions (Gasser et al., 2006; Haskett et al., 2010; Holzapfel et al., 2000). Results in Table 5 show limit strains needed for fibre straightening in the direction of uniaxial load; the values for fibres arranged in two helical fibre families are approximately two times higher than for wavy fibres with the same maximum angle.

While higher fibre alignment under uniaxial load in their direction is highly expectable, it is not so under equibiaxial extension. Figure S1 shows clearly that with stretches equal in all directions no reason for reorientation of helical fibres exists and they should be elongated (and thus bear the load) from the very beginning. As it is evidently not the case and the fibre alignment increases similarly with uniaxial and equibiaxial stretch, the results support the hypothesis of a single family of wavy fibres. These tendencies were confirmed for both types of distributions by statistically significant differences between the equibiaxially loaded and unloaded specimens, as well as by non-significant differences between equibiaxial and circumferentially dominated load or between unloaded specimens and axially dominated load. Moreover, the strains at the toe region of the stress–strain curve are typically between 10 % and 20 % (Azadani et al., 2012; Lisický et al., 2021) and correspond much better to the strains needed for full straightening of wavy fibres (see Table 1). In contrast, the stiffness of the tissue with two helical (and waveless) fibre families should be much higher from the very beginning of equibiaxial extension under which no rotation is induced. As it is not the case (see, for instance, (Peña et al., 2015)), all of these results support the hypothesis on one family of wavy fibres.

There are some other studies applying similar concepts of evaluation of fibre directions in arterial wall under deformation. For instance, (Schrauwen et al., 2012) carried out histological analyses at different levels of inner pressure in the arterial adventitia and showed similar tendency of increasing concentration parameters for both in-plane and out-of-plane angles. (Gaul et al., 2017) used Small Angle Light Scattering for detection of fibre directions in the specimens, either unloaded or under uniaxial tension in the dominant fibre direction. They found higher concentration of fibres under load and one fibre family in intima and media, while two fibre families were declared in adventitia. However, the results in Figure 5 in (Gaul et al., 2017) show that these two fibre families come from tissue non-homogeneity and the histograms could be better interpreted as only one axially oriented fibre family.

Table 5
Limit strain values (engineering) for both geometric models with different angles of fibres.

Model	$\alpha = \pm 40^\circ$	$\alpha = \pm 45^\circ$	$\alpha = \pm 50^\circ$
Two waveless helical fibre families	0.31	0.41	0.56
One family of wavy (sinusoidal) fibres	0.16	0.22	0.29

The authors declare that they have no known competing financial interests or personal relationships that could have appeared to influence the work reported in this paper.

While most applied methods investigate local orientations (Morrill et al., 2016; Rezakhaniha et al., 2012; Schriefl et al., 2013), only few studies aim at global fibre directions (Ayyalasomayajula et al., 2019). Consequently, prevailing histological results show two or more fibre families arranged symmetrically close to the circumferential direction (Baek et al., 2007; Hu et al., 2007; Schriefl et al., 2013; Schriefl, Zeindlinger, et al., 2012). However, the results determined by using manual methods may be skewed by small amount of evaluated data (Finlay et al., 1995; Gasser et al., 2012; Schriefl, Zeindlinger, et al., 2012; Wicker et al., 2008). Furthermore, histograms determined on unloaded (or only slightly stretched) samples with wavy fibres appear similar to two fibre families (Gasser et al., 2012; Schriefl, Zeindlinger, et al., 2012). (Schriefl et al., 2013) lean towards two families in adventitia and intima and one circumferential family in media direction. Their data were obtained using SHG from confocal microscope images of specimens under constant axial prestress and pressure. Thus, they were also not capable to evaluate the extension-related changes in fibre orientation. On the other side, (Polzer et al., 2015) analysed the distribution of collagen fibres across the thickness of the unloaded aortic wall and found, similarly to this study, circumferentially aligned fibres in intima and media, with a gradual transition to almost isotropic fibre distribution in the adventitia.

The authors who fitted all the parameters of HGO or GOH models to mechanical test data only, i.e. without histological information, obtained mostly two directions at approx. $\pm 45^\circ$ in individual layers, as presented in (Fischer et al., 2023; Gasser et al., 2006; Haskett et al., 2010; Holzapfel et al., 2000; Schriefl, Reinisch, et al., 2012). These results occur typically in TA, while in TM the fibres incline toward circumferential direction (Haskett et al., 2010; Holzapfel et al., 2000, 2002). However, only one study supports this orientation histologically: in human aortic intima and media, (Schriefl, Reinisch, et al., 2012) found two fibre families being highly symmetric ($+39.4^\circ / -39.6^\circ$). In contrast, the same group (Schriefl et al., 2013) confirmed existence of one fibre family in human aortic media (circumferential) and intima (axial). From the same experiments they proposed two fibre families in adventitia but the evidence is rather weak; the fibres in adventitia are oriented in several different directions in the sublayers throughout its thickness and they could be fitted with one circumferential fibre family with a similar (not very high) accuracy.

To mention limitations of this study, some of them are intrinsic for the PLM method applied in our histological analyses. Unfortunately, due to the need of thin tissue slices, it does not enable to trace the collagen fibres and to evaluate their waviness and global directions. The specimens may also be distorted when positioned on the glass plate. Although the specimen orientation is strictly kept, inaccuracies of several degrees may occur due to slice curvature especially with narrow slices. These inaccuracies may explain the deviations of the mean fibre orientation from the circumferential direction in the order of units of degrees. In contrast to high accuracy of strain evaluation, we were not capable to ensure equibiaxial strain preciously. Nevertheless, if significant differences exist between the groups (see Table 4) in spite of their broad dispersion, surely these differences would be even more pronounced for more homogeneous groups. Morover, our automated algorithm for evaluation of fibre directions made the procedure fully operator independent and enabled large datasets independent of the selection of

evaluated regions (Novák et al., 2015).

The results of our study show that one family of dominantly circumferential wavy fibres coincides much better with the experimental findings, mechanical as well as histological. Although there are studies using methods of fluorescent microscopy (multiphoton + SHG, confocal etc.) (Niestrawska et al., 2022; Rezakhaniha et al., 2012; Schrauwen et al., 2012; Sugita & Matsumoto, 2017) and thus capable to assess fibre dispersion as well as their waviness (Ayyalasomayajula et al., 2019; Niestrawska et al., 2022; Wan et al., 2012), none of them analyzed mutual relations between fibre waviness and local and global fibre directions. Thus this relation remains an important issue for future research to transform rigorously the histological results into parameters of structure-based constitutive models considering fibre waviness and their global directions in the unloaded state. To explain all discrepancies and to confirm our hypothesis, a comprehensive analysis evaluating the waviness of fibres together with dispersion in their global orientation is prepared in near future using human aortic tissues.

5. Conclusion

The histological analyses of porcine aortas under load have shown the mean orientation of fibres as dominantly circumferential and independent on the load. In circumferential-axial plane the distributions of local directions appeared either bimodal or unimodal but an increasing alignment (~lower dispersion) of collagen fibre local orientations occurred under tissue extension. The quantitative comparison showed the concentration parameter (~alignment) increased with circumferential stretch which indicates that the potential bi-modality of the analysed distribution is related to fibre waviness rather than to their dispersion. This hypothesis is confirmed even more by the observed increase of the concentration parameter with equibiaxial deformation because equibiaxial stretches cannot induce any fibre rotation. Such result is also supported by insignificant differences of the angle between both fibre families under equibiaxial and uniaxial (in the dominant fibre direction) extension. All of these findings dispute the existence of two helical fibre families interpreted from bimodal distributions; these interpretations are mostly based on *local* fibre orientations while structure-based constitutive models are defined through their *global* orientations.

CRediT authorship contribution statement

Michaela Turčanová: Writing – original draft, Visualization, Methodology, Investigation, Data curation, Formal analysis, Resources. **Jiří Fischer:** Resources, Investigation, Formal analysis. **Markéta Hermanová:** Supervision, Conceptualization. **Zdeněk Bednařík:** Writing – review & editing, Methodology, Investigation, Formal analysis. **Pavel Skácel:** Writing – review & editing, Software, Methodology, Conceptualization. **Jiří Burša:** Funding acquisition, Writing – review & editing, Supervision, Project administration.

Declaration of competing interest

The authors declare that they have no known competing financial interests or personal relationships that could have appeared to influence the work reported in this paper.

Acknowledgement

This work was supported by Czech Science Foundation project No. 21-21935S.

Appendix A. Supplementary material

Supplementary data to this article can be found online at https://doi.org/10.1016/j.jbiomech.2023.111868.

References

Agianniotis, A., Rezakhaniha, R., Stergiopulos, N., 2011. A structural constitutive model considering angular dispersion and waviness of collagen fibres of rabbit facial veins. Biomed. Eng. Online 10, 1–17. https://doi.org/10.1186/1475-925X-10-18.

Akyildiz, A.C., Speelman, L., Gijsen, F.J.H., 2014. Mechanical properties of human atherosclerotic intima tissue. J. Biomech. 47 (4) https://doi.org/10.1016/j.jbiomech.2014.01.019.

Ayyalasomayajula, V., Pierrat, B., Badel, P., 2019. A computational model for understanding the micro-mechanics of collagen fiber network in the tunica adventitia. Biomech. Model. Mechanobiol. 18 (5), 1507–1528. https://doi.org/10.1007/s10237-019-01161-1.

Azadani, A.N., Chitsaz, S., Matthews, P.B., Jaussaud, N., Leung, J., Tsinman, T., Ge, L., Tseng, E.E., 2012. Comparison of Mechanical Properties of Human Ascending Aorta and Aortic Sinuses. Ann. Thorac. Surg. 93 (1), 87–94. https://doi.org/10.1016/J.ATHORACSUR.2011.08.002.

Baek, S., Gleason, R.L., Rajagopal, K.R., Humphrey, J.D., 2007. Theory of small on large: Potential utility in computations of fluid-solid interactions in arteries. Comput. Meth. Appl. Mech. Eng. 196 (31–32), 3070–3078. https://doi.org/10.1016/j.cma.2006.06.018.

Ferruzzi, J., Vorp, D.A., Humphrey, J.D., 2011. On constitutive descriptors of the biaxial mechanical behaviour of human abdominal aorta and aneurysms. J. R. Soc. Interface 8 (56), 435–450. https://doi.org/10.1098/rsif.2010.0299.

Finlay, H. M., McCullough, L., & Canham, P. B. (1995). *Three-Dimensional Collagen Organization of Human Brain Arteries at Different Transmural Pressures* (pp. 301–312). http://www.jvascsurg.org/citationdownload.

Finlay, H.M., Whittaker, P., Canham, P.B., 1998. Collagen organization in the branching region of human brain arteries. Stroke 29 (8), 1595–1601.

Fischer, J., & Bursa, J. (2019). Comparison of Various Distributions Used for Collagen Fibre Orientations in Arterial Layers. *Engineering Mechanics 2019*, *May*, 113–116. 10.21495/71-0-113.

Fischer, J., Turčanová, M., Man, V., Hermanová, M., Bednařík, Z., & Burša, J. (2023). Importance of experimental evaluation of structural parameters for constitutive modelling of aorta. *Journal of the Mechanical Behavior of Biomedical Materials*, *138* (August 2022), 105615. 10.1016/j.jmbbm.2022.105615.

Gasser, T.C., Ogden, R.W., Holzapfel, G.A., 2006. Hyperelastic modelling of arterial layers with distributed collagen fibre orientations. J. R. Soc. Interface 3 (6), 15–35. https://doi.org/10.1098/rsif.2005.0073.

Gasser, T.C., Gallinetti, S., Xing, X., Forsell, C., Swedenborg, J., Roy, J., 2012. Spatial orientation of collagen fibers in the abdominal aortic aneurysm's wall and its relation to wall mechanics. Acta Biomater. 8 (8), 3091–3103. https://doi.org/10.1016/j.actbio.2012.04.044.

Gaul, R.T., Nolan, D.R., Lally, C., 2017. Collagen fibre characterisation in arterial tissue under load using SALS. J. Mech. Behav. Biomed. Mater. 75 (July), 359–368. https://doi.org/10.1016/j.jmbbm.2017.07.036.

Geest, J. P. Vande, Sacks, M. S., & Vorp, D. A. (2006). The effects of aneurysm on the biaxial mechanical behavior of human abdominal aorta. *Journal of Biomechanics*, *39* (7), 1324–1334.

Grytz, R., Meschke, G., 2009. Constitutive modeling of crimped collagen fibrils in soft tissues. J. Mech. Behav. Biomed. Mater. 2 (5), 522–533. https://doi.org/10.1016/j.jmbbm.2008.12.009.

Guinier, A., Fournet, G., & Yudowitch, K. L. (1955). *Small-angle scattering of X-rays*.

Haskett, D., Johnson, G., Zhou, A., Utzinger, U., Vande Geest, J., 2010. Microstructural and biomechanical alterations of the human aorta as a function of age and location. Biomech. Model. Mechanobiol. 9 (6), 725–736. https://doi.org/10.1007/s10237-010-0209-7.

Hoffman, A. H., Louis, S., Woodard, P. K., Louis, S., Billiar, K. L., & Wang, L. (2017). *Stiffness Properties of Adventitia , Media , and Full Thickness Human Atherosclerotic Carotid Arteries in the Axial and Circumferential Directions*. 10.1115/1.4037794.

Holzapfel, G. A., Niestrawska, J. A., Ogden, R. W., Reinisch, A. J., & Schriefl, A. J. (2015). *Modelling non-symmetric collagen fibre dispersion in arterial walls*. 10.1098/rsif.2005.0073.

Holzapfel, G.A., Gasser, C.T., Ogden, R.W., 2000. A New Constitutive Framework for Arterial Wall Mechanics and a Comparative Study of Material Models. J. Elast. 61, 1–48. https://doi.org/10.1023/A:1010835316564.

Holzapfel, G.A., Stadler, M., Schulze-Bauer, C.A.J., 2002. A layer-specific three-dimensional model for the simulation of balloon angioplasty using magnetic resonance imaging and mechanical testing. Ann. Biomed. Eng. 30 (6), 753–767. https://doi.org/10.1114/1.1492812.

Hu, J.J., Baek, S., Humphrey, J.D., 2007. Stress-strain behavior of the passive basilar artery in normotension and hypertension. J. Biomech. 40 (11), 2559–2563. https://doi.org/10.1016/j.jbiomech.2006.11.007.

Jett, S.V., Hudson, L.T., Baumwart, R., Bohnstedt, B.N., Mir, A., Burkhart, H.M., Holzapfel, G.A., Wu, Y., Lee, C.H., 2020. Integration of polarized spatial frequency domain imaging (pSFDI) with a biaxial mechanical testing system for quantification of load-dependent collagen architecture in soft collagenous tissues. Acta Biomater. 102, 149–168. https://doi.org/10.1016/j.actbio.2019.11.028.

Lanir, Y., 1983. Constitutive equations for fibrous connective tissues. J. Biomech. 16 (1), 1–12. https://doi.org/10.1016/0021-9290(83)90041-6.

Lisický, O., Hrubanová, A., Staffa, R., Vlachovský, R., Burša, J., 2021. Constitutive models and failure properties of fibrous tissues of carotid artery atheroma based on their uniaxial testing. J. Biomech. 129 https://doi.org/10.1016/j.jbiomech.2021.110861.

Low, J.C.M., Ober, T.J., McKinley, G.H., Stankovic, K.M., 2015. Quantitative polarized light microscopy of human cochlear sections. Biomed. Opt. Express 6 (2), 599. https://doi.org/10.1364/boe.6.000599.

Marino, M., von Hoegen, M., Schröder, J., Wriggers, P., 2018. Direct and inverse identification of constitutive parameters from the structure of soft tissues. Part 1: micro- and nanostructure of collagen fibers. Biomech. Model. Mechanobiol. 17 (4), 1011–1036. https://doi.org/10.1007/s10237-018-1009-8.

Martufi, G., Gasser, T.C., 2011. A constitutive model for vascular tissue that integrates fibril, fiber and continuum levels with application to the isotropic and passive properties of the infrarenal aorta. J. Biomech. 44 (14), 2544–2550. https://doi.org/10.1016/j.jbiomech.2011.07.015.

Morrill, E.E., Tulepbergenov, A.N., Stender, C.J., Lamichhane, R., Brown, R.J., Lujan, T. J., 2016. A validated software application to measure fiber organization in soft tissue. Biomech. Model. Mechanobiol. 15 (6), 1467–1478. https://doi.org/10.1007/s10237-016-0776-3.

Niestrawska, J.A., Pukaluk, A., Babu, A.R., Holzapfel, G.A., 2022. Differences in Collagen Fiber Diameter and Waviness between Healthy and Aneurysmal Abdominal Aortas. Microsc. Microanal. 1–15 https://doi.org/10.1017/S1431927622000629.

Novák, K., Polzer, S., Tichý, M., Burša, J., 2015. Automatic Evaluation of Collagen Fiber Directions from Polarized Light Microscopy Images. Microsc. Microanal. 21 (4), 863–875. https://doi.org/10.1017/S1431927615000586.

Peña, J.A., Martínez, M.A., Peña, E., 2015. Layer-specific residual deformations and uniaxial and biaxial mechanical properties of thoracic porcine aorta. J. Mech. Behav. Biomed. Mater. 50, 55–69. https://doi.org/10.1016/j.jmbbm.2015.05.024.

Polzer, S., Gasser, T.C., Novák, K., Man, V., Tichý, M., Skácel, P., Burša, J., 2015. Structure-based constitutive model can accurately predict planar biaxial properties of aortic wall tissue. Acta Biomater. 14, 133–145.

Polzer, S., Gasser, T.C., Vlachovský, R., Kubíček, L., Lambert, L., Man, V., Novák, K., Slažanský, M., Burša, J., Staffa, R., 2020. Biomechanical indices are more sensitive than diameter in predicting rupture of asymptomatic abdominal aortic aneurysms. J. Vasc. Surg. 71 (2), 617–626.e6. https://doi.org/10.1016/j.jvs.2019.03.051.

Rezakhaniha, R., Agianniotis, A., Schrauwen, J.T.C., Griffa, A., Sage, D., Bouten, C.V.C., Van De Vosse, F.N., Unser, M., Stergiopulos, N., 2012. Experimental investigation of collagen waviness and orientation in the arterial adventitia using confocal laser scanning microscopy. Biomech. Model. Mechanobiol. 11 (3–4), 461–473. https://doi.org/10.1007/s10237-011-0325-z.

Rowe, A.J., Finlay, H.M., Canham, P.B., 2003. Collagen biomechanics in cerebral arteries and bifurcations assessed by polarizing microscopy. J. Vasc. Res. 40 (4), 406–415.

Sáez, P., García, A., Peña, E., Gasser, T.C., Martínez, M.A., 2016. Microstructural quantification of collagen fiber orientations and its integration in constitutive modeling of the porcine carotid artery. Acta Biomater. 33, 183–193. https://doi.org/10.1016/j.actbio.2016.01.030.

Sassani, S.G., Kakisis, J., Tsangaris, S., Sokolis, D.P., 2015. Layer-dependent wall properties of abdominal aortic aneurysms: experimental study and material characterization. J. Mech. Behav. Biomed. Mater. 49, 141–161.

Schrauwen, J.T.C., Vilanova, A., Rezakhaniha, R., Stergiopulos, N., van de Vosse, F.N., Bovendeerd, P.H.M., 2012. A method for the quantification of the pressure dependent 3D collagen configuration in the arterial adventitia. J. Struct. Biol. 180 (2), 335–342. https://doi.org/10.1016/j.jsb.2012.06.007.

Schriefl, A.J., Reinisch, A.J., Sankaran, S., Pierce, D.M., Holzapfel, G.A., 2012a. Quantitative assessment of collagen fibre orientations from two-dimensional images of soft biological tissues. J. R. Soc. Interface 9 (76), 3081–3093. https://doi.org/10.1098/rsif.2012.0339.

Schriefl, A.J., Zeindlinger, G., Pierce, D.M., Regitnig, P., Holzapfel, G.A., 2012b. Determination of the layer-specific distributed collagen fibre orientations in human thoracic and abdominal aortas and common iliac arteries. J. R. Soc. Interface 9 (71), 1275–1286. https://doi.org/10.1098/rsif.2011.0727.

Schriefl, A.J., Wolinski, H., Regitnig, P., Kohlwein, S.D., Holzapfel, G.A., 2013. An automated approach for three-dimensional quantification of fibrillar structures in optically cleared soft biological tissues. J. R. Soc. Interface 10 (80). https://doi.org/10.1098/rsif.2012.0760.

Sugita, S., Matsumoto, T., 2017. Multiphoton microscopy observations of 3D elastin and collagen fiber microstructure changes during pressurization in aortic media. Biomech. Model. Mechanobiol. 16 (3), 763–773. https://doi.org/10.1007/s10237-016-0851-9.

Tsamis, A., Phillippi, J.A., Koch, R.G., Pasta, S., D'Amore, A., Watkins, S.C., Wagner, W. R., Gleason, T.G., Vorp, D.A., 2013. Fiber micro-architecture in the longitudinal-radial and circumferential-radial planes of ascending thoracic aortic aneurysm media. J. Biomech. 46 (16), 2787–2794.

Turčanová, M., Hrtoň, M., Dvořák, P., Novák, K., Hermanová, M., Bednařík, Z., Polzer, S., Burša, J., 2021. Full-Range Optical Imaging of Planar Collagen Fiber Orientation Using Polarized Light Microscopy. Biomed Res. Int. 2021 https://doi.org/10.1155/2021/6879765.

Wan, W., Dixon, J.B., Gleason, R.L., 2012. Constitutive modeling of mouse carotid arteries using experimentally measured microstructural parameters. Biophys. J . 102 (12), 2916–2925. https://doi.org/10.1016/j.bpj.2012.04.035.

Wicker, B.K., Hutchens, H.P., Wu, Q., Yeh, A.T., Humphrey, J.D., 2008. Normal basilar artery structure and biaxial mechanical behaviour. Comput. Meth. Biomech. Biomed. Eng. 11 (5), 539–551. https://doi.org/10.1080/10255840801949793.